

## Effect of Ni Doping into ZnO Nanostructures for Structural, Morphological, Electrical, and Gas Sensing Properties

In this chapter, the impact of Ni doping into ZnO nanostructures on structural, morphological, electrical, and hydrogen gas sensing performance will be described. Different concentration of Ni is doped into ZnO to detect extremely low concentration (1 ppm) of hydrogen at mild operating temperature of 75°C. Ni doping exceptionally increases the sensing response and decrease the operating temperature of the sensor than undoped ZnO. The main role of the Ni-doping is to produce more active sites for chemisorbed oxygen on the sensor's surface and, correspondingly, upgrade the sensing response. In addition, the gas sensing mechanism will be discussed in the end of this chapter.

### 4.1 INTRODUCTION

Doping of transition metal element into  $MO_x$  is one of the eminent factors which improve the sensing response of  $MO_x$  sensor. Transition metals like Ni, Co, Fe and Cu have been mostly used as dopants into  $MO_x$  [Zhang *et al.*, 2017; Maswanganye *et al.*, 2017; Bai *et al.*, 2014; Gong *et al.*, 2006]. Dopants not only modify the resistance but also increase the sensing response of  $MO_x$  sensor. These metal dopants also play a vital role in decreasing the operating temperature of the gas sensor, and improving selectivity, stability, and response time for target gas molecules. It has been noticed that the surface morphology of  $MO_x$  changes after doping the metal elements into it. The grain size of doped  $MO_x$  nanostructures becomes smaller as compared to pure  $MO_x$  nanostructures, which is due to further restrictions of movement of crystallites during the interaction of boundaries between the dopant and the host material [Maciel *et al.*, 2003]. Therefore, the growth of crystal stops because of introduction of dopant element. Gas sensing response can be enhanced by using small-sized particles having high surface area; resulting in the enhancement of large number of chemisorbed oxygen ions and increased barrier height. Keeping in mind this motivation, ZnO, has been used as a host material in this work because it is one of the most favorable  $MO_x$  [Kobrinsky *et al.*, 2008; Zhu *et al.*, 2005]. Performance of the ZnO-based gas sensors is largely affected by the dimension of nanostructures of a sensing layer and operating temperature [Ranwa *et al.*, 2014]. Li *et al.* [Li *et al.*, 2014], grew  $TiO_2$  nanotubes doped with 8% Ni which shows a maximum sensing response of ~24% and ~65% to 2% hydrogen at RT and 200°C, respectively. Authors in [Yang *et al.*, 2015] investigated the 2 at% Cd doped ZnO nanorods grown by hydrothermal method that was able to sense 500 ppm of  $H_2$  gas at operating temperature ranging from 50°C to 100°C. Liu *et al.*, reported Mg-doped ZnO thin films exhibiting gas sensing response ( $R_a/R_g$ ) for about 1.7 to 5 ppm  $H_2$  at 150°C [Liu *et al.*, 2011]. Sett *et al.* [Sett *et al.*, 2017], synthesized Co-doped ZnO nanorods and then characterized them within the range of 1000 to 3000 ppm  $H_2$ . The sensing response was outstanding for ZnO with 8 mol% of Co, and showed ~3 times better sensitivity for 3000 ppm of  $H_2$  gas at 300°C as compared to undoped ZnO. Shen *et al.* [Shen *et al.*, 2009] synthesized undoped and Pd-doped  $SnO_2$  nanowires and exhibited a reversible response to  $H_2$  gas at operating temperatures between RT and 300°C. Sensor based on 2 wt% Pd doped  $SnO_2$  nanowires revealed an excellent response of ~253 to 1000 ppm of  $H_2$  gas at 100°C.

This chapter demonstrates highly sensitive Ni-doped ZnO sensor which is able to detect extremely low concentration of hydrogen at mild operating temperature (75°C). The operating

temperature for this sensor is much lower than previous reports in literature ( $>150^{\circ}\text{C}$ ). ZnO has been doped with 0%, 2%, 4% and 6% of Ni, using RF magnetron sputtering system and then gas sensing response has been carried out for hydrogen gas sensing response with respect to the operating temperature (RT to  $150^{\circ}\text{C}$ ).

## 4.2 EXPERIMENTAL SETUP

Undoped and Ni-doped ZnO nanostructures have been grown on p-Si (100) substrate by using an RF sputtering system. A ZnO target (99.99% purity) is utilized for the deposition under Ar gas environment. Ni chips ( $3\times 3\text{ mm}^2$ ) were also attached on ZnO target to get the desired doping concentration of Ni (2, 4, and 6%) into the ZnO lattice, as shown in Figure 4.1. Sputtering parameters such as substrate temperature, RF power, and substrate to target distance were fixed at  $600^{\circ}\text{C}$ , 50W and 5cm, respectively. The deposition has been done in 2 h at  $1.5\times 10^{-2}$  mbar chamber pressure with an Ar flow of 25 sccm. Surface morphology and structural analyses of the undoped and Ni-doped ZnO were carried out using field emission scanning electron microscopy (FESEM, JSM 7100F, Jeol) and an X-ray diffractometer (XRD, Bruker D8 Advance), respectively. CL studies have been carried out at room temperature using CL spectroscopy apparatus (MONO CL4, Gatan) installed with scanning electron microscope (JSM-7100F, JEOL). Therefore, circular shaped aluminum (Al) electrodes having diameter of  $400\mu\text{m}$  have been fabricated on ZnO-based nanostructures by using thermal evaporation system with the help of shadow mask.

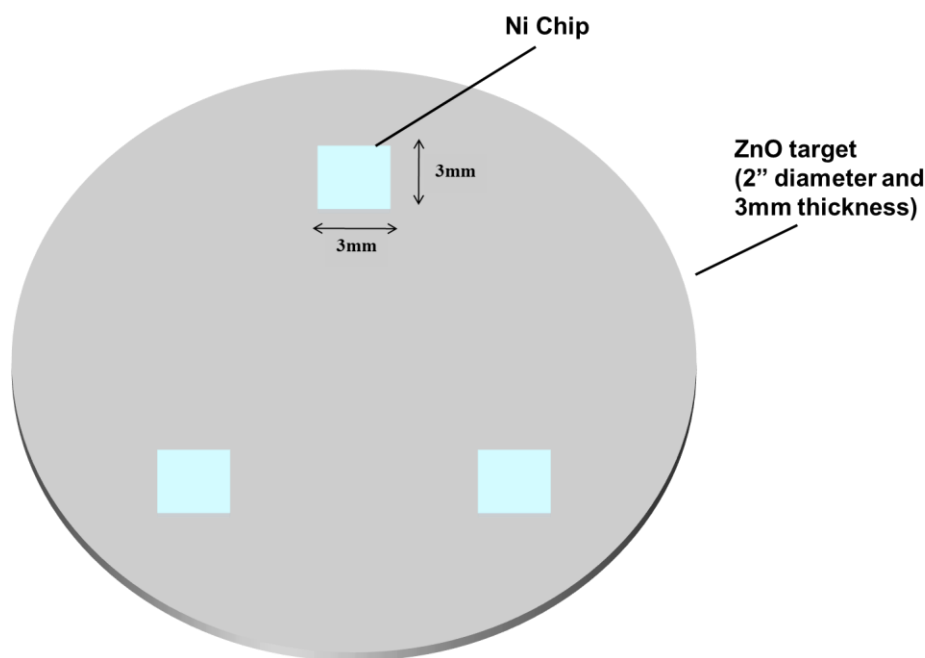


**Figure 4.1:** Schematic diagram of ZnO target

A gas sensing setup has been used to detect 1% hydrogen in pure argon environment using semiconductor characterization system (SCS- 4200, Keithley). 10% RH in sensing chamber has been maintained during gas sensing measurements. A constant operating voltage (3V) is applied to the sensor during the measurement, and sensor's resistance response curve has been taken out via  $I$ - $V$  characteristics. Thereafter, hydrogen sensing measurements have been performed at the operating temperature ranging from RT to  $150^{\circ}\text{C}$ . For ppm level of hydrogen detection, pre-calibrated volume of 1% hydrogen gas in Ar is introduced into sensing chamber by using gas tight syringe.

### 4.3 STRUCTURAL CHARACTERIZATION

Figure 4.2 (a-d) shows the XRD pattern of undoped and Ni-doped ZnO nanostructures deposited on p-Si (100) substrate. XRD pattern of undoped ZnO reveals a strong (002) peak related to the hexagonal wurtzite structure along with highly orientated c-axis [Zhang *et al.*, 2017].

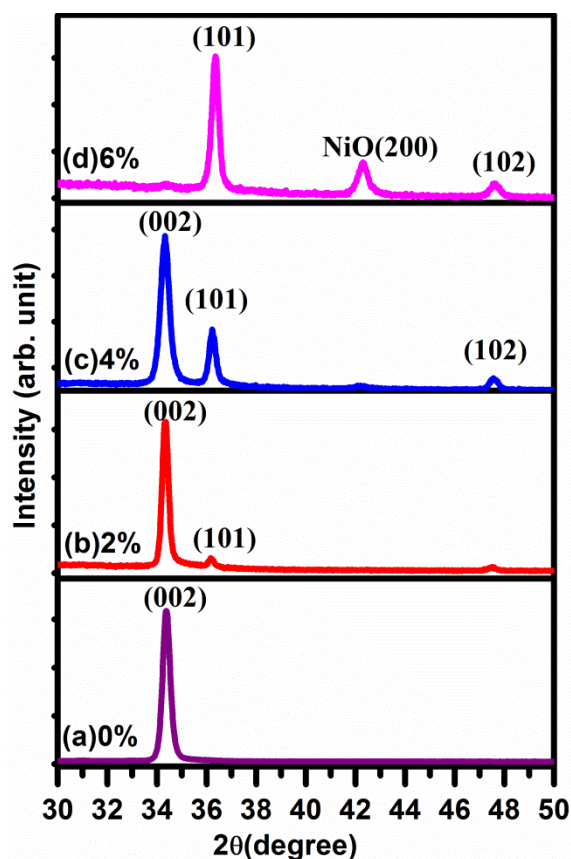


**Figure: 4.2** XRD pattern of (a) undoped, (b) 2% Ni- doped, (c) 4% Ni- doped and (d) 6% Ni- doped ZnO nanostructures

Other planes such as (101) and (102) have been observed with increased peak intensity as doping concentration increases from 2 to 4% Ni into ZnO. No other peaks are found corresponding to NiO or Ni, which depict the substitution of Zn<sup>+2</sup> ions (0.074 nm) by Ni<sup>+2</sup> ions (0.069 nm) [Bouaoud *et al.*, 2013]. Upon further addition of Ni doping to 6%, (002) peak of ZnO vanishes and a small peak can be seen at  $2\theta = 42.33^\circ$  corresponding to NiO which indicates the existence of NiO phase with ZnO [Long *et al.*, 2014]. The removal of (002) peak of 6% Ni is caused by lattice distortion and degraded crystallinity of ZnO nanostructures along the c- axis. This degraded crystallinity might be due to the different ionic radii of Zn and Ni ions which generates stress and creates crystal deformation. Tsay *et al.* [Tsay *et al.*, 2012] has investigated that 5% Ga doped ZnO did not show the (002) peak in XRD spectra, thus indicating the degraded crystallinity of Ga doped ZnO thin films.

### 4.4 FILM MORPHOLOGY

Effect of Ni doping on morphology of ZnO has been investigated by using FESEM. Figure 4.3 (a-h) depicts top view as well as cross sectional view of undoped (2, 4, and 6%), and Ni- doped ZnO nanostructures, respectively.

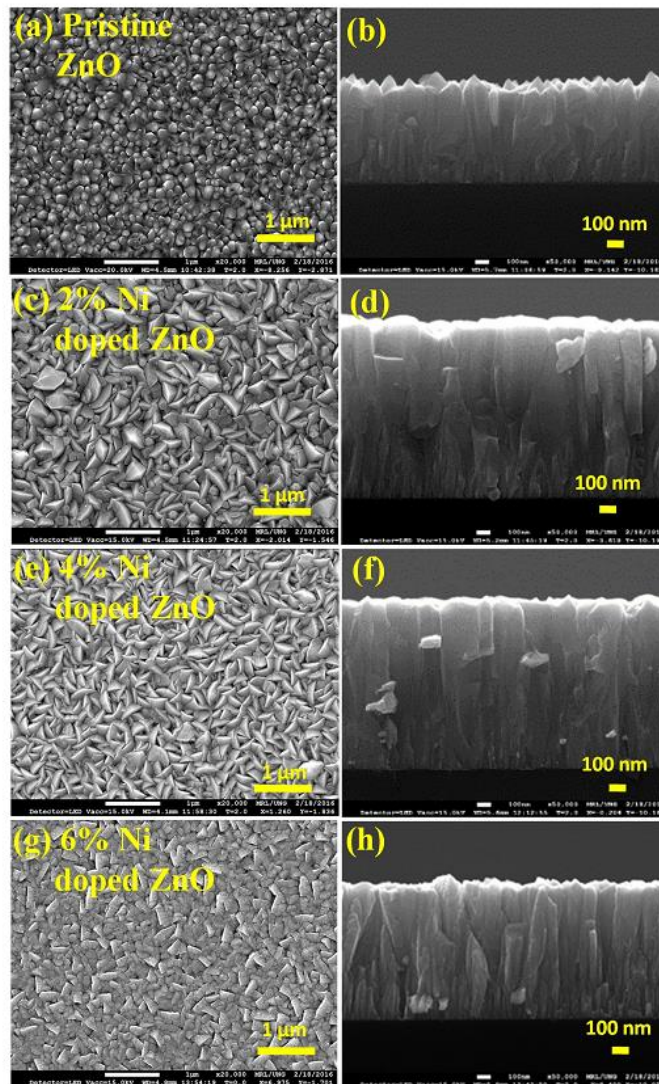


**Figure 4.3:** (a-h) Top view and cross sectional view of FESEM images for (a-b) undoped, (c-d) 2% Ni- doped, (e-f) 4% Ni- doped and (g-h) 6% Ni- doped ZnO nanostructures

Undoped ZnO nanostructures represent columnar structure along the conical tips of highly dense packed ZnO nanorods uniformly deposited throughout the substrate as shown in Figure 4.3 (a). However, the surface morphology of ZnO nanostructures has been transformed with increasing concentration of Ni. When Ni dopant is introduced into ZnO, conical tips of ZnO nanostructures transform into nanoplates (Figure 4.3 (c-e)). Here, XRD spectra also prove the change in the preferred orientation of the deposited film induced by Ni-doping. The columnar structure with nanoplates morphology is present in 2% and 4% Ni doped ZnO; while for the 6% Ni, columnar structure with rectangular surface can be observed in FESEM images. The amounts of Ni doping ( $2\pm 0.1$ ,  $4\pm 0.1$ , and  $6\pm 0.1$  %) in ZnO have been confirmed by EDX quantitative analysis which can be seen in Figure 4.4.

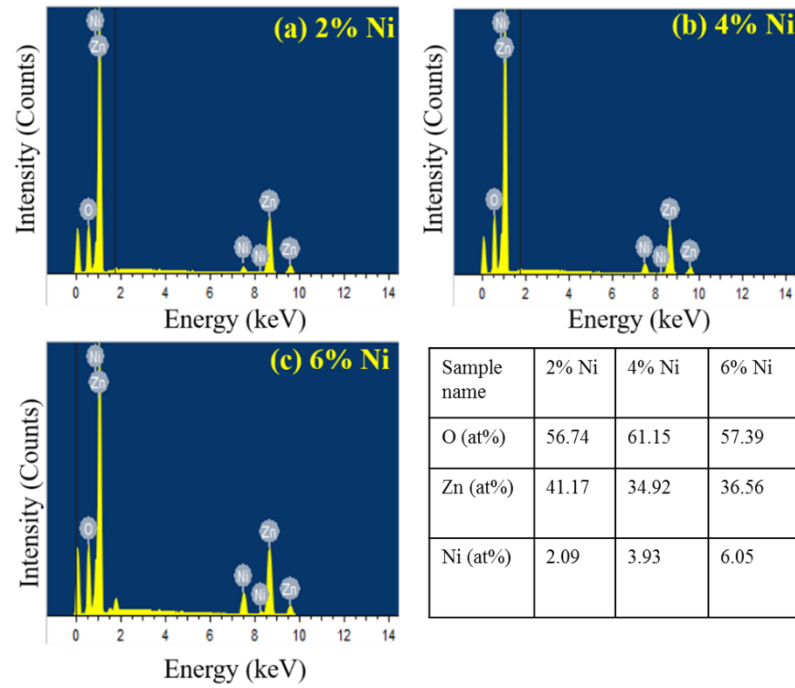


Figure 4.4: (a-c) EDX spectra of 2%, 4%, and 6% Ni-doped ZnO nanostructures, respectively

#### 4.5 OPTICAL PROPERTIES

CL characterization of undoped and 4% Ni-doped ZnO nanostructures at room temperature reveals a clear picture about crystallinity and structural defects in Figure 4.5.

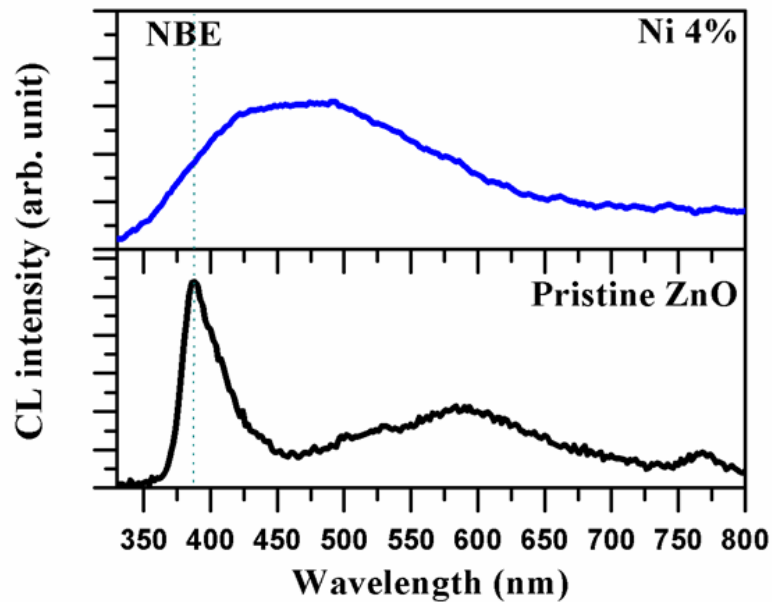
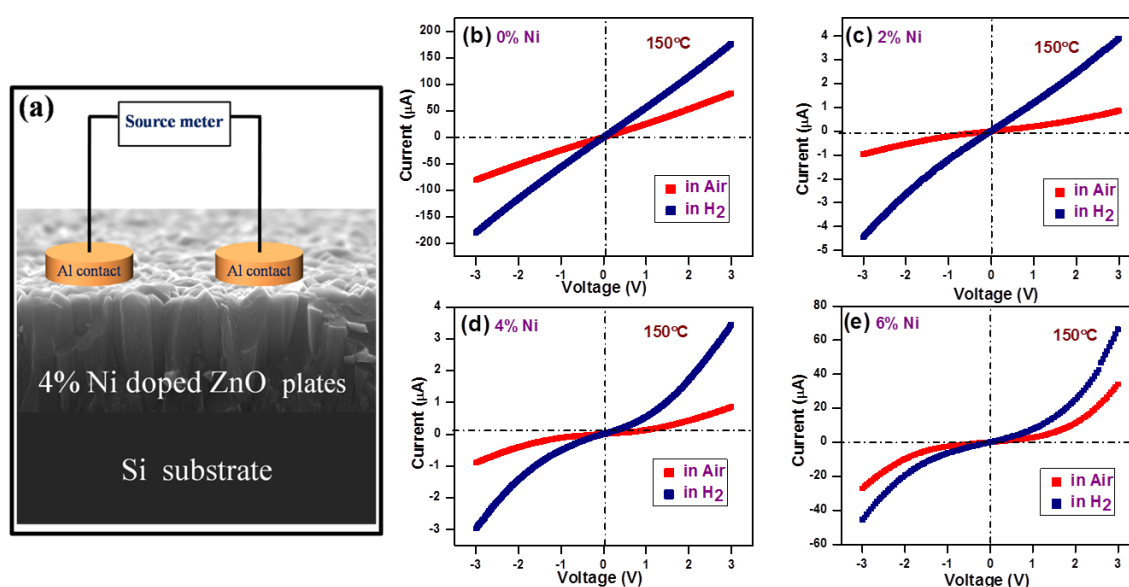


Figure 4.5: CL spectra of undoped and 4% Ni-doped ZnO nanostructures at RT

Undoped ZnO reveals a strong NBE peak at  $\sim 385$  nm which confirms the crystalline growth of ZnO nanostructures. Moreover, 4% Ni-doped ZnO nanostructures suggest the presence of a broad peak at 400-700 nm with respect to undoped ZnO. This wide band emission region shows the presence of structural defects like oxygen vacancies ( $V_o$ ), interstitial defects, and antisite oxygen ( $O_{zn}$ ) that might have existed in 4% Ni-doped ZnO nanostructures [Abbasi *et al.*, 2014].

## 4.6 ELECTRICAL CHARACTERIZATION

Current conduction mechanism of Ni-doped ZnO nanostructures based sensor has been described using electrical characterization techniques. Figure 4.6 (a) and 4.6 (b-e) represents the schematic diagram of device and their Current-Voltage ( $I$ - $V$ ) characteristics in air and 1%  $H_2$  at  $150^\circ C$ , respectively. Initially, undoped ZnO nanostructure with Al contacts shows ohmic behaviour in air and  $H_2$  gas. Higher current has been observed in presence of hydrogen, attributed to decrease in depletion width of chemisorbed oxygen ions on ZnO nanostructures surface [Ranwa *et al.*, 2015]. On the other hand, 4% Ni-doped ZnO having columnar structure of nanoplates surface revealing rectifying behavior, which also indicates that the current of the Ni-doped ZnO sensor decreases from hundreds of micro ampere to few micro amperes than undoped ZnO. This is caused by the presence of higher barrier height between metal and ZnO as well as between the columnar structures of nanoplates shape in 4% Ni-doped ZnO sample, attributed to large change in resistance in air and hydrogen environment than undoped ZnO.



**Figure 4.6** (a) Schematic diagram of Sensor device, (b-e)  $I$ - $V$  characteristics of undoped, 2% Ni-doped, 4% Ni-doped, and 6% Ni-doped, ZnO nanostructure in presence of air as well as 1% hydrogen at  $150^\circ C$

It is observed that the sensor current in sensor increases in air in 6% Ni-doped ZnO. The higher current might be due to change in growth direction of ZnO and generation of more defects at higher dopant concentration of Ni. Separation of NiO (p-type) from ZnO (n-type) has been initiated in 4% Ni-doped ZnO (clearly seen in XRD spectra), which further became higher in 6% Ni-doping. Herein, the  $I$ - $V$  characteristics of the Ni-doped ZnO nanostructures are strongly affected by the ratio of p-n heterojunction to the ZnO barrier. If this ratio is too high, then the relative change in current of sensor will be significantly low because of less reaction between chemisorbed oxygen ions and target gas [Zhiming *et al.*, 2012]. The relative change in current has been maximized at the optimum condition when the ratio of p-n heterojunction to the ZnO barrier is balanced. This ratio was found suitable for 4% Ni. Further adding of Ni dopant upto 6% leads to enhancement in the p-n heterojunction and decrease in the total number of ZnO barriers. Consequently, the p-n heterojunction became highly dominated at higher content of Ni doping, and the current conduction decreases at this amount. Moreover, the  $I$ - $V$  characterization of 4% Ni-doped ZnO is also evident for optimum condition of the ratio of p-n heterojunction to ZnO barrier, and shows large change in ZnO barrier height in presence of air to hydrogen gas than 6% Ni-doped ZnO.

## 4.7 HYDROGEN SENSING MEASUREMENT

In  $\text{MO}_x$  based gas sensors, gas sensing is basically a surface phenomenon. The key factors like operating temperature, gas concentration, and doping amount strongly influence the sensing response. Relative response of the gas sensor can be calculated by relative change in resistance in air and analyzed gas. Sensor response at 1% for hydrogen has been studied from RT to 150 °C. Figure 4.7 (a-d) shows the relative response of gas sensor for undoped, 2, 4, and 6% Ni- doped ZnO nanostructures. It can be observed that the operating temperature has significant impact on the sensor's response. Relative response of undoped ZnO sensor increases from ~3.5% to 43.4% for 1%  $\text{H}_2$  gas when temperature increases from RT to 150 °C. Moreover, there is also a significant improvement in sensor's response for Ni doped films, whereas 4% Ni dopant increases from ~10% to 68.8%, which is approximately ~1.5 times larger than the undoped ZnO. Further enhancement in Ni doping decrease sensor response as compared to undoped ZnO nanostructures based sensor.

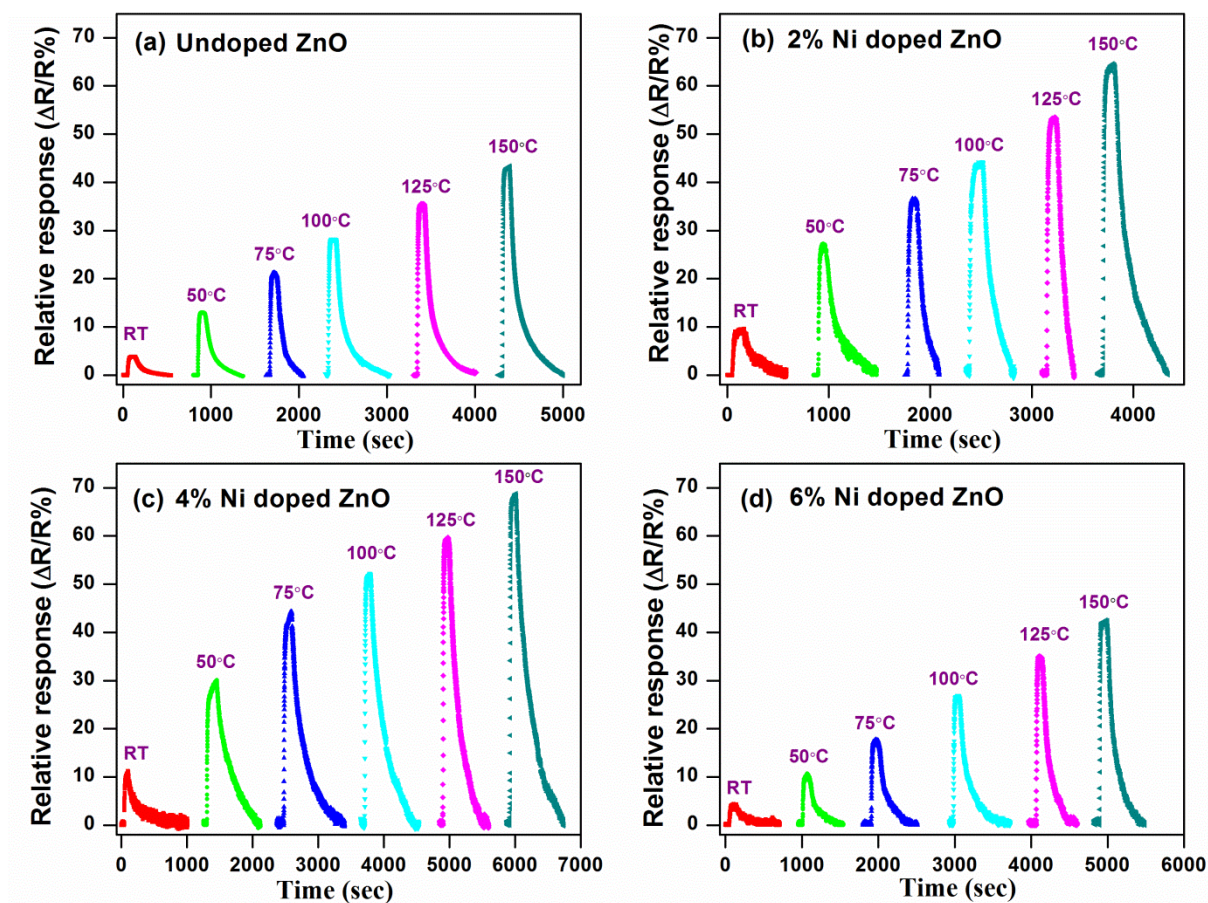


**Figure 4.7:** Gas sensor relative response for undoped, 2%, 4%, and 6% Ni- doped ZnO nanostructures with increasing operating temperature ranging from RT to 150°C for 1% hydrogen concentration

The comparison of relative response for all sensors at 150°C is shown in Figure 4.8. Maximum relative response ~68.8% has been observed by 4% Ni- doped ZnO nanostructures than undoped ZnO nanostructure (~43.4%). Further addition of Ni doping up to 6% decreases the sensor relative response to ~42.3%, which is almost similar to undoped ZnO nanostructure.

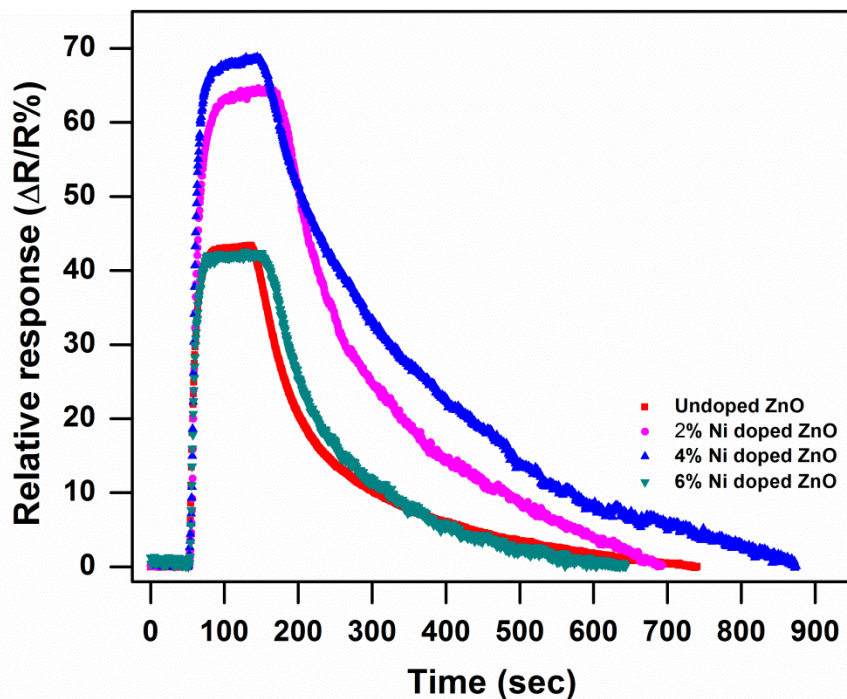


Figure 4.8: Relative response of undoped and Ni- doped ZnO nanostructures based sensor at 150°C

Long-term stability test is also a crucial factor for gas sensors in real market applications [Korotcenkov *et al.*, 2011]. Figure 4.9 shows long-term stability curve for 4% Ni-doped ZnO nanoplates where the sensing measurement has been tested up to 150 days in 1% hydrogen at 150 °C.

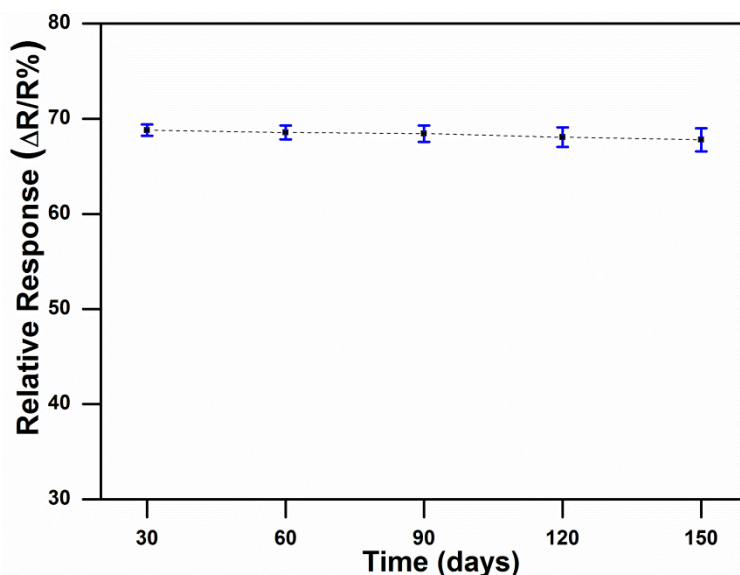


Figure 4.9: Long term stability curve of 4% Ni-doped ZnO nanoplates for 150 days

It has been observed that the relative response is stable with time. The hydrogen gas detection in ppm level is also possible for this sensor at moderate operating temperature. Figure 4.10 shows the relative response of 4% Ni-doped ZnO based sensor with increasing hydrogen concentration from 1ppm to 100 ppm at moderate operating temperature of 75 °C. Sensor's response has been observed to be ~10% for 1ppm of hydrogen. With increasing hydrogen concentration from 1ppm to 100 ppm, sensor response increases from ~10% to ~22.12%. It is also observed that the increase in hydrogen concentrations leads to decrease in the sensor's response time from few hundreds of second to few second.



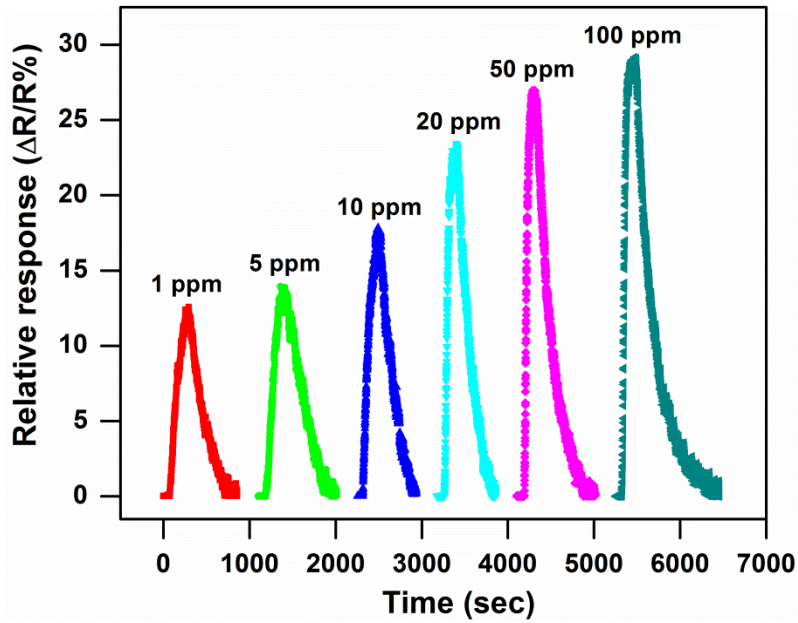


Figure 4.10: 4% Ni- doped ZnO based sensor relative response with increasing hydrogen concentration from 1ppm to 100 ppm at 75 °C

#### 4.8 CALCULATION OF ACTIVATION ENERGY

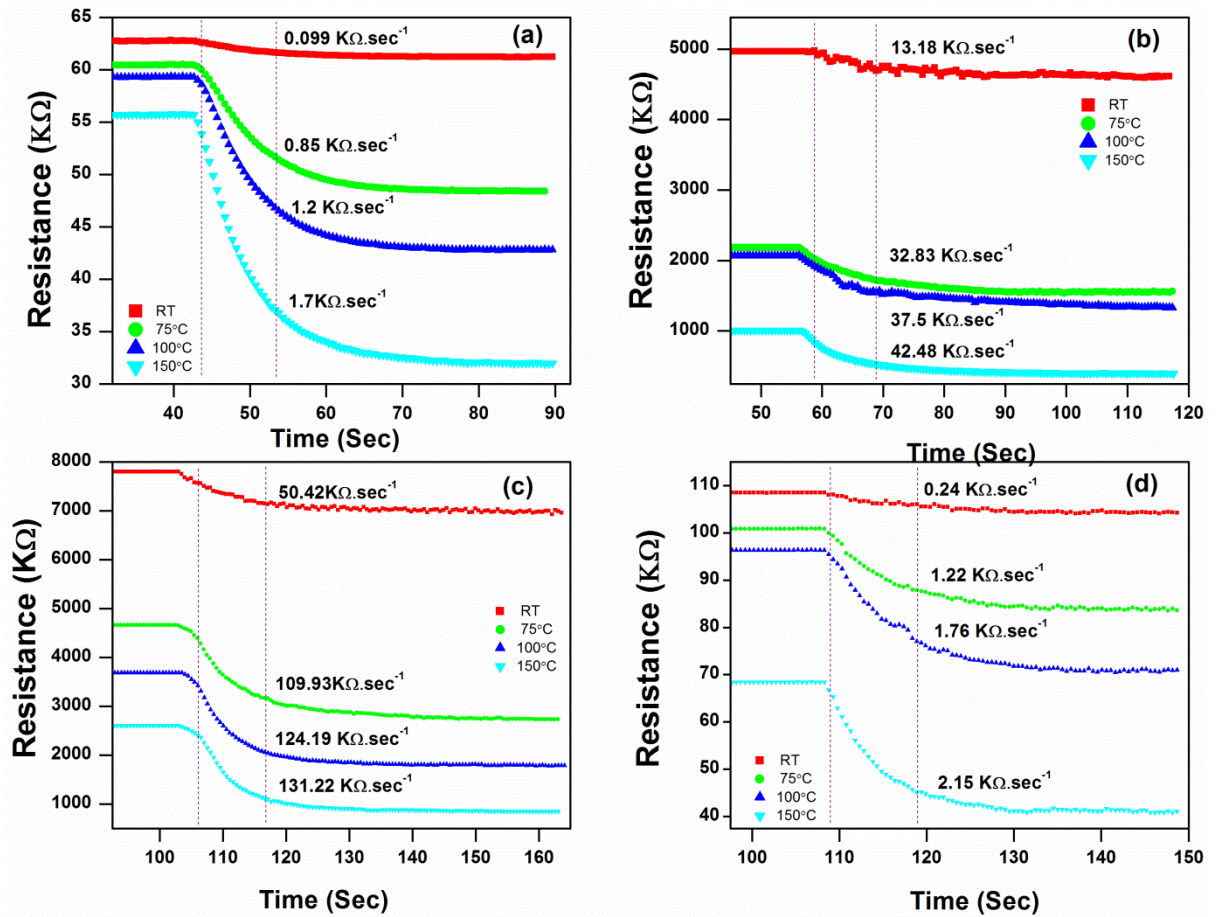


Figure 4.11: (a-d) Temperature dependent resistance v/s time curve for undoped, 2%, 4%, and 6% Ni- doped ZnO nanostructures based sensor on exposure of 1% hydrogen with operating temperature ranging from RT to 150 °C

In order to compute adsorption activation energy for 1% hydrogen gas; first of all temperature dependent resistance v/s time curves have been plotted for all the samples, which can be seen in Figure 4.11 (a-d).

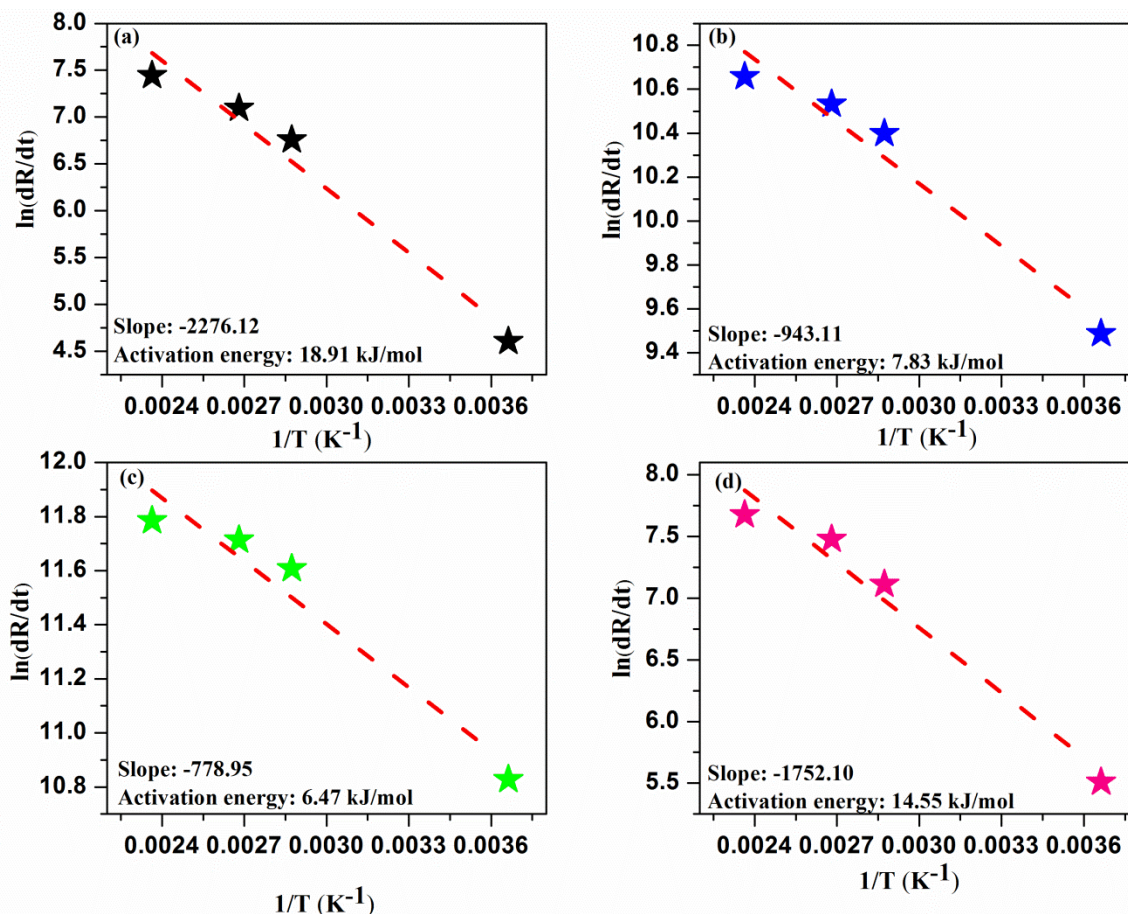


Figure 4.12: (a-d) Rate of change in resistance with temperature for undoped, 2%, 4%, and 6% Ni- doped ZnO nanostructures, respectively

Calculated activation energy has been observed to be 18.91kJ/mol, 7.83kJ/mol, 6.47 kJ/mol, and 14.56kJ/mol for undoped, 2% Ni, 4% Ni, and 6% Ni- doped ZnO nanostructures, respectively in Figure 4.13.

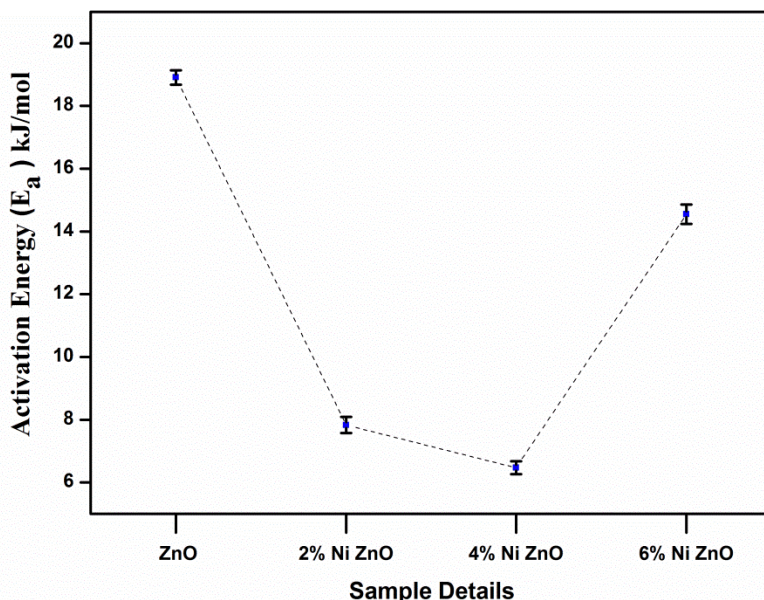
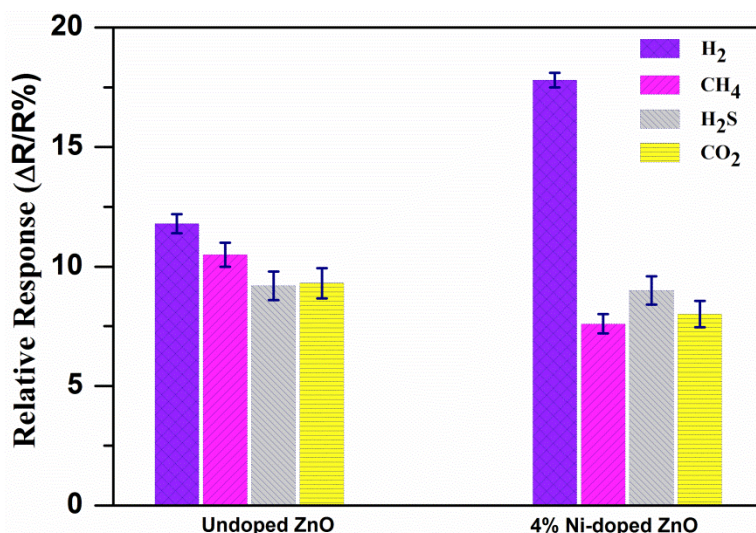


Figure 4.13: Activation energy plot for undoped and Ni- doped ZnO nanostructures

For selectivity test, the relative response of hydrogen gas has been compared with other reactive gases like CH<sub>4</sub>, H<sub>2</sub>S, and CO<sub>2</sub>. Figure 4.14 shows the selectivity histogram for undoped ZnO and 4% Ni doped ZnO nanostructures based sensor for 5ppm of H<sub>2</sub>, CH<sub>4</sub>, H<sub>2</sub>S, and CO<sub>2</sub> gases at 150 °C.



**Figure 4.14:** Selectivity test of different target gases for 5 ppm concentration at 150°C operating temperature

Undoped ZnO nanostructure based sensor does not show selectivity for 5ppm hydrogen gas concentration as compared to other reactive gases. In contrast to undoped ZnO nanostructure based sensor, 4% Ni doped ZnO nanostructure exhibits a remarkable H<sub>2</sub> response (~ 17.8 %) with a weak response (~ 7.4 for 9.11%) for other gases. This validates the selectivity of the sensor towards hydrogen gas even at lowest gas concentration (5ppm).

A comparison of sensing performance of several sensors for hydrogen with different morphology and transition metal doping has been listed in Table 4.1. While making comparison with other reported doped ZnO sensors, RF sputtered Ni doped ZnO nanostructures manifest moderate sensor response even at lower working temperature range.

**Table 4.1:** Comparison of hydrogen sensing performance of various metal doped ZnO sensors

Sl No.	Sample	H <sub>2</sub> concentration (ppm)	Working temperature (°C)	Response (S)	Reference
1	ZnO p-n homojunction	1000	400	1.15 <sup>a</sup>	Hazra et al., 2006
2	1D ZnO nano-assemblies	5000	400	12 <sup>a</sup>	Barreca et al., 2010
3	Mg doped ZnO film	5000	300	50 <sup>a</sup>	Liu et al., 2011
4	Co- doped ZnO nanorods	3000	150	53.7% <sup>c</sup>	Sett et al., 2017
5	Cr- doped ZnO nanowhiskers	100	37	47 <sup>a</sup>	Renitta et al., 2016

6	ZnO nanobelt	10000	385	14.3 <sup>a</sup>	Sadek <i>et al.</i> , 2007
7	rGO/ZnO composite	200	150	3.5 <sup>a</sup>	Anand <i>et al.</i> , 2014
8	In -doped ZnO thin film	1	350	5% <sup>b</sup>	Pati <i>et al.</i> , 2015
9	Pd decorated ZnO nanosponge	20000	20	82 <sup>a</sup>	Zhao <i>et al.</i> , 2015
10	Cd doped ZnO nanorods	500	150	2.6 <sup>d</sup>	Yang <i>et al.</i> , 2015
11	Ni doped ZnO nanostructures	10000 5	150 150	69% <sup>b</sup> 17.77% <sup>b</sup>	This work

$$^a S = R_a/R_g, ^b S = (R_a - R_g)/R_a \times 100\%, ^c S = (I_g - I_a)/I_a \times 100\%, ^d S = R_{N_2}/R_g$$

The sensor is able to detect 5 ppm hydrogen concentration having 17.7% sensor response at 150 °C due to doping. Hence, these optimized Ni doped ZnO nanostructures are efficient enough to sense lowest amount of hydrogen concentration (1 ppm, 5 ppm) at mild temperature ranging from (RT to 150 °C) with high selectivity towards hydrogen as compared to other samples. Highest relative sensor response for 4% Ni- doped ZnO sensor is due to lowest adsorption activation energy which leads to fast adsorption/desorption reaction on the sensor's surface along with large change in the depletion region of the sensor. Hence, it is very obvious from the relative response curve that Ni content greatly increases the sensing response and reduces the operating temperature of the sensor down to 75°C than undoped ZnO. Moreover, the major role of Ni doping is to produce more active sites for chemisorbed oxygen on the sensor's surface, and correspondingly enhance its sensing response [Zhao *et al.*, 2011; Lin *et al.*, 2017].

#### 4.9 GAS SENSING MECHANISM

In addition to gas sensing mechanism for MO<sub>x</sub> materials, the sensing response of Ni-doped ZnO based sensors are strongly dependent upon the rate of adsorption of oxygen ions. This is also affected by operating temperature. Once chemisorbed oxygen ions are adsorbed on Ni-doped ZnO, hydrogen releases free electrons to the conduction band of ZnO nanostructures during exposure to hydrogen. Therefore, the sensor's resistance and depletion region reduces. The sensor's response is strongly correlated with the adsorption activation energy, Ni concentration, hydrogen concentration, and presence of active site. Gas sensing (adsorption/desorption of oxygen) properties of MO<sub>x</sub> have been highly affected by surface area as well as structural defects. As the Ni doping concentration increases up to 4% in ZnO nanostructures, surface area increases due to the transformation of nano-grain structures in undoped ZnO into nano-plates with increased surface area. This might be one of the causes of enhancement in sensor's response for 4% Ni doped ZnO nanostructures. The other key factors for increased number of active sites may be related to structural defects (clearly seen in CL). Here, structural defects act as active sites and charge transfer to adsorbed oxygen ions leading to more hydrogen reactions. Thus, 4% Ni doped ZnO nanostructures reveal highest sensor response as compared to undoped ZnO nanostructures.

4% Ni-doped ZnO makes tremendous enhancement in relative response which may be due to the following factors: (i) Number of active sites for adsorption of oxygen ions increases the thickness of depletion layer by giving more amount of electrons from conduction band of Ni-doped ZnO nanostructures (ii) lower activation energy enhances adsorption/desorption reaction kinetics to 4% Ni-doped ZnO nanoplates which results in the enhancement of current due to reduction in barrier height during exposure to H<sub>2</sub> gas. On the other hand, 6% Ni doping displays a decrease in relative response because of the change in growth direction of ZnO as well as its degraded crystallinity. Apart from this, the activation energy has been found to be higher than 4% Ni-doped ZnO, causing less adsorption/desorption reaction on the sensor's surface and decrease in the relative response.

#### **4.10 CONCLUSION**

In the conclusion of this chapter, undoped and Ni doped (2, 4, and 6% Ni) ZnO nanostructures have been deposited by RF magnetron sputtering system. XRD pattern reveals hexagonal wurtzite structure for undoped and Ni-doped ZnO. In undoped ZnO, preferential growth is observed along with the c-axis. Secondary phase of NiO has been detected for 6% Ni-doped ZnO. FESEM shows the columnar structure having conical tips of very dense packed ZnO nanorods for undoped ZnO nanostructures. However, the surface morphology transforms with the Ni doping. High resistance of 4% Ni- doped ZnO is due to higher barrier height between metal and ZnO as well as between columnar structures having the shape of nanoplates. The highest relative response is observed for 4% Ni-doped ZnO nanostructures. Lower limit of detection is also possible down to 1ppm (~10%) at moderate operating temperature (75 °C) and the stability sustains up to 150 days without reduction in relative response for 4% Ni-doped ZnO sensor. Excellent relative response is observed for 4% Ni-doped ZnO sensor, caused by large surface sites for adsorption of oxygen on nanoplates, and lowest activation energy ~6.47 KJ/mol. Lastly, the reduction in relative response for 6% Ni- doped ZnO is due to the modification in growth direction of ZnO crystal structures.

